nanomaterials

MDPI

Article

Non-Additive Optical Response in Transition Metal Dichalcogenides Heterostructures

Marwa A. El-Sayed [1,2], Andrey P. Tselin [1,3], Georgy A. Ermolaev [1], Mikhail K. Tatmyshevskiy [1], Aleksandr S. Slavich [1], Dmitry I. Yakubovsky [1], Sergey M. Novikov [1], Andrey A. Vyshnevyy [1], Aleksey V. Arsenin [1] and Valentyn S. Volkov [1,*]

1 Center for Photonics and 2D Materials, Moscow Institute of Physics and Technology, 9 Institutsky Lane, Dolgoprudny 141700, Russia
2 Department of Physics, Faculty of Science, Menoufia University, Shebin El-Koom 32511, Egypt
3 Photonics and Quantum Materials Department, Skolkovo Institute of Science and Technology, 3 Nobel, Moscow 143026, Russia
* Correspondence: volkov.vs@mipt.ru; Tel.: +7-926-735-93-98

Abstract: Van der Waals (vdW) heterostructures pave the way to achieve the desired material properties for a variety of applications. In this way, new scientific and industrial challenges and fundamental questions arise. One of them is whether vdW materials preserve their original optical response when assembled in a heterostructure. Here, we resolve this issue for four exemplary monolayer heterostructures: MoS_2/Gr, MoS_2/hBN, WS_2/Gr, and WS_2/hBN. Through joint Raman, ellipsometry, and reflectance spectroscopies, we discovered that heterostructures alter MoS_2 and WS_2 optical constants. Furthermore, despite the similarity of MoS_2 and WS_2 monolayers, their behavior in heterostructures is markedly different. While MoS_2 has large changes, particularly above 3 eV, WS_2 experiences modest changes in optical constants. We also detected a transformation from dark into bright exciton for MoS_2/Gr heterostructure. In summary, our findings provide clear evidence that the optical response of heterostructures is not the sum of optical properties of its constituents.

Keywords: transition-metal dichalcogenides; two-dimensional materials; optical constants; heterostructure; refractive index; nanophotonics; spectroscopic ellipsometry

Citation: El-Sayed, M.A.; Tselin, A.P.; Ermolaev, G.A.; Tatmyshevskiy, M.K.; Slavich, A.S.; Yakubovsky, D.I.; Novikov, S.M.; Vyshnevyy, A.A.; Arsenin, A.V.; Volkov, V.S. Non-Additive Optical Response in Transition Metal Dichalcogenides Heterostructures. *Nanomaterials* **2022**, *12*, 4436. https://doi.org/10.3390/nano12244436

Academic Editors: Giancarlo Soavi and Ioannis Paradisanos

Received: 13 November 2022
Accepted: 9 December 2022
Published: 13 December 2022

1. Introduction

The foundation of contemporary solid state physics and the industry is semiconductor heterostructures [1,2]. They offer a unique opportunity to manipulate fundamental material parameters such as bandgap width [3,4], charge carrier mobilities [5,6], and refractive index [7,8]. However, the majority of heterostructures are produced by expensive and complex epitaxial growth [9,10], which is also limited to mixing crystals with less than 1% lattice misfit [11]. On the other hand, dangling bond-free surfaces and van der Waals (vdW) forces enable unrestricted stacking of two-dimensional (2D) materials [12–14], which can be controlled via microspectroscopy [15,16]. In electrical and optoelectronic applications, vdW heterostructures have already demonstrated their great value [17–20]. For instance, graphene (Gr) on top of hexagonal boron nitride (hBN) demonstrates record-breaking carrier mobility of over 10^5 $cm^2V^{-1}s^{-1}$ [21,22]. Additionally, 2D materials can be placed at various orientation angles, providing an indispensable degree of freedom to further adjust the properties of vdW materials [23–26]. Among the greatest examples are band structure modification [27,28], interlayer excitons [29,30], and unconventional superconductivity in magic-angle graphene superlattices [31,32]. The use of vdW heterostructures for optical engineering has also been suggested by recent theoretical research [33–36]. Several studies have also reported that when Gr is included in heterostructures, its intrinsic absorption can grow by up to 60% [37,38]. These results raise the fundamental question of non-additive

optical effects in heterostructures (Figure 1a). In other words, we can utilize pristine optical constants of 2D materials [39,40] in vdW heterostructures.

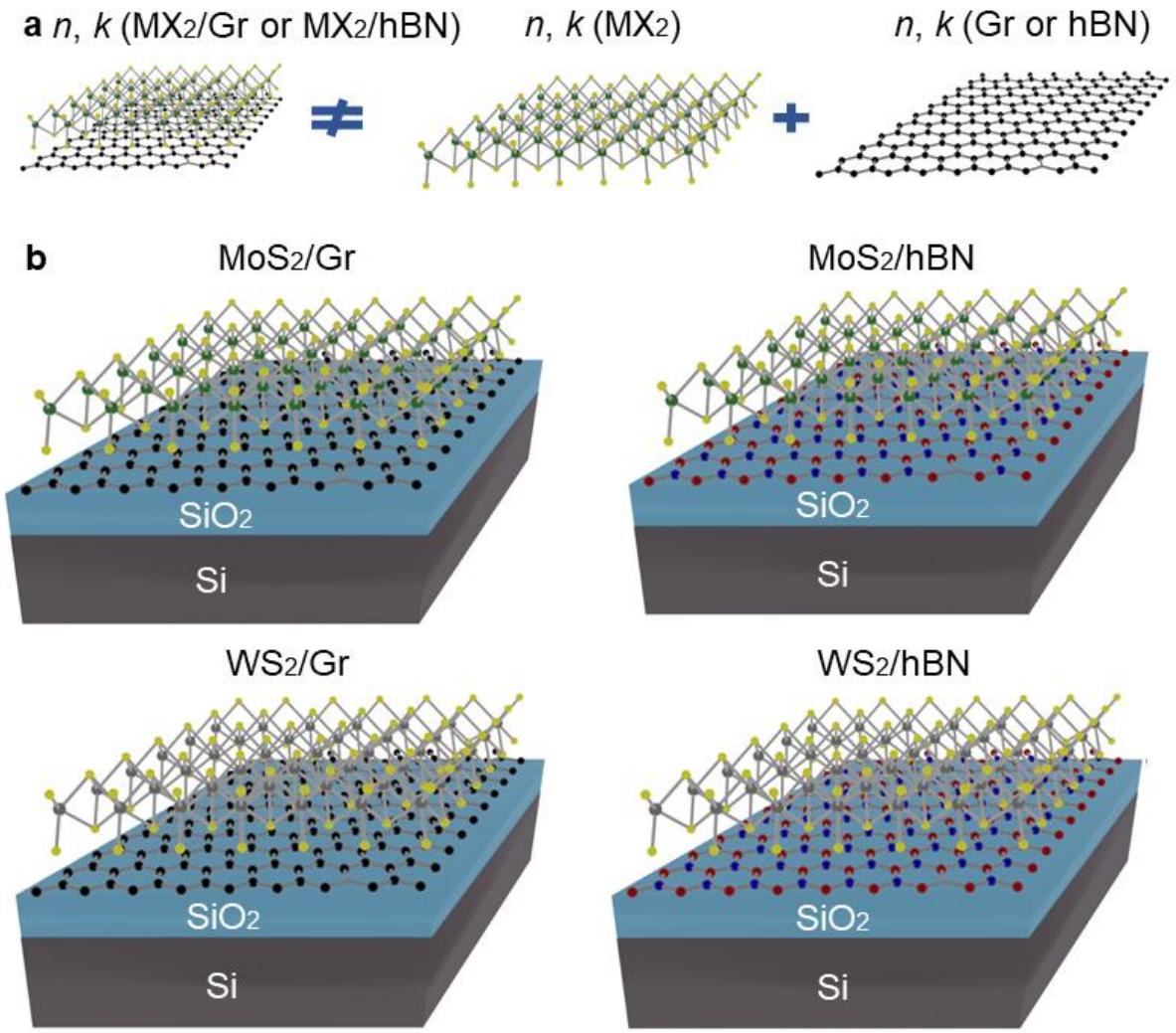

Figure 1. (**a**) Schematic illustration of non-additive optical response of heterostructures. (**b**) Heterostructures used in the work: MoS_2/Gr, MoS_2/hBN, WS_2/Gr, and WS_2/hBN. All vdW materials are single layers. Green, grey, yellow, black, red, and blue circles label Mo, W, S, C, B, and N atoms, respectively.

In this study, we investigated this issue for four exemplary heterostructures, depicted schematically in Figure 1b: MoS_2/Gr, MoS_2/hBN, WS_2/Gr, and WS_2/hBN. We discovered that non-additive effects arise in vdW heterostructures. Still, the change in optical constants strongly depends on the constituents of the heterostructures.

2. Materials and Methods

2.1. Materials

Full area coverage two-dimensional heterostructures of MoS_2/Gr, MoS_2/hBN, WS_2/Gr, and WS_2/hBN were purchased from SixCarbon (6Carbon Technology, Shenzhen, China), where monolayers of MoS_2, WS_2, graphene and hBN were grown via chemical vapor deposition (CVD) method [41], and subsequently, monolayers of each material were transferred using the standard water-assisted method [42] to form the desired heterostructures on a Si wafer substrate with silicon dioxide.

2.2. Raman Characterization

Horiba LabRAM HR Evolution confocal scanning Raman microscope (Horiba Ltd., Kyoto, Japan) was employed for acquisition of the Raman spectra of heterostructures. All measurements were carried out under linearly polarized excitation at free space wavelengths of 532 nm with a 1800 lines/mm diffraction grating and a ×100 objective with 0.90 numerical aperture. The spot diameter was approximately 0.9 μm. The Raman spectra were recorded at an incident laser power of 1.75 mW and an integration time of 10 s. At least 10 spectra were collected from each sample.

2.3. Spectroscopic Ellipsometry Characterization

Spectroscopic ellipsometer (VASE, J.A. Woollam Co., Lincoln, NE, USA) was used to determine optical constants of transition metal dichalcogenides (MoS_2 and WS_2) in heterostructures. For ellipsometry spectra analysis, we used WVASE software and described the heterostructure with a four-layer optical model (from bottom to top): Si substrate, SiO_2, Gr or hBN, and MoS_2 or WS_2. Optical constants for Si, SiO_2, Gr, and hBN were taken from previous research [43–45]. The thicknesses of SiO_2 layers are 11.9, 11.8, 317.9, and 328.0 nm for MoS_2/Gr, MoS_2/hBN, WS_2/Gr, and WS_2/hBN heterostructures, respectively. At the same time, optical response of MoS_2 and WS_2 was modeled as a sum of Tauc-Lorentz (TL) oscillators with varied parameters. The formula for the imaginary part of the TL oscillator dielectric permittivity ε_2 reads as [46,47]:

$$\varepsilon_2 = \begin{cases} \frac{1}{E} \cdot \frac{AE_0C\left(E-E_g\right)^2}{\left(E^2-E_0^2\right)^2+C^2E^2} & \text{for } E > E_g \\ 0 & \text{for } E < E_g \end{cases} \quad (1)$$

where E is the photon energy, A is the oscillator strength, C is the oscillator broadening, E_g is the optical bandgap, and E_0 is the oscillator central energy, while the real part ε_1 of the dielectric function is derived from Kramers–Kronig integration plus ε_∞ to account for high energy electronic transitions.

2.4. Reflectance Measurements

The spectroscopic reflection measurements were performed in the 1.65–2.48 eV (500–750 nm) spectral range on a reflectometer FTPadv integrated into the spectroscopic ellipsometer Sentech SE 800E (SENTECH Instruments GmbH, Berlin, Germany). The reflected light was collected in a backscattering configuration using a focused objective. We measured the reference and background radiation using the supplied reference sample (silicon wafer with 3 nm silicon dioxide). Then, the reflection data were collected from the sample.

3. Results and Discussion

3.1. Non-Additive Optical Effects in Phonon Spectra

In contrast to previous research [48–50] on exfoliated samples with small lateral dimensions of about 10 μm, we focused on large-scale vdW heterostructures since they are more likely to satisfy the demands of practical applications. With this intention, our samples were synthesized via chemical vapor deposition (CVD) [41] and then wet-transferred [42] on each other to form the desired heterostructures (Figure 1) with lateral sizes of around 1×1 cm^2. Furthermore, CVD-grown crystals have random orientations of crystallographic axes [51], which lead to a random distribution of orientation angles between top and bottom monolayers. Hence, the interaction between layers in our vdW heterostructures is averaged over the orientation angle. To investigate the impact of interlayer interaction on optical properties of 2D materials, we performed spectroscopic ellipsometry [40,52,53] and Raman spectroscopy [54,55] measurements.

According to Raman measurements (Figure 2a), MoS_2/Gr and MoS_2/hBN heterostructures exhibit a noticeable difference in MoS_2 spectra. For MoS_2/Gr heterostructure, the $E^1{}_{2g}$

mode has a tiny blue shift by 0.5 cm^{-1}, whereas the A_{1g} mode red shifted by 1 cm^{-1}, in comparison with MoS_2/hBN heterostructure (Figure 2a). We also included in Figure 1a the Raman spectrum of the MoS_2 monolayer on a standard silicon dioxide (SiO_2) substrate as a reference. Predictably, this spectrum is closer to MoS_2/hBN than to MoS_2/Gr because SiO_2 and hBN are both dielectrics, while Gr is semimetal. Based on the difference between the positions of the Raman peaks, we concluded that MoS_2 optical constants should have some change in the MoS_2/hBN heterostructure, compared to the classical MoS_2/SiO_2, and even greater modification is anticipated for the MoS_2/Gr heterostructure. Conversely, Raman spectra of WS_2 do not change in all three cases (Figure 1b). Therefore, we expected minimal changes in WS_2 optical constants in the WS_2/Gr and WS_2/hBN heterostructures.

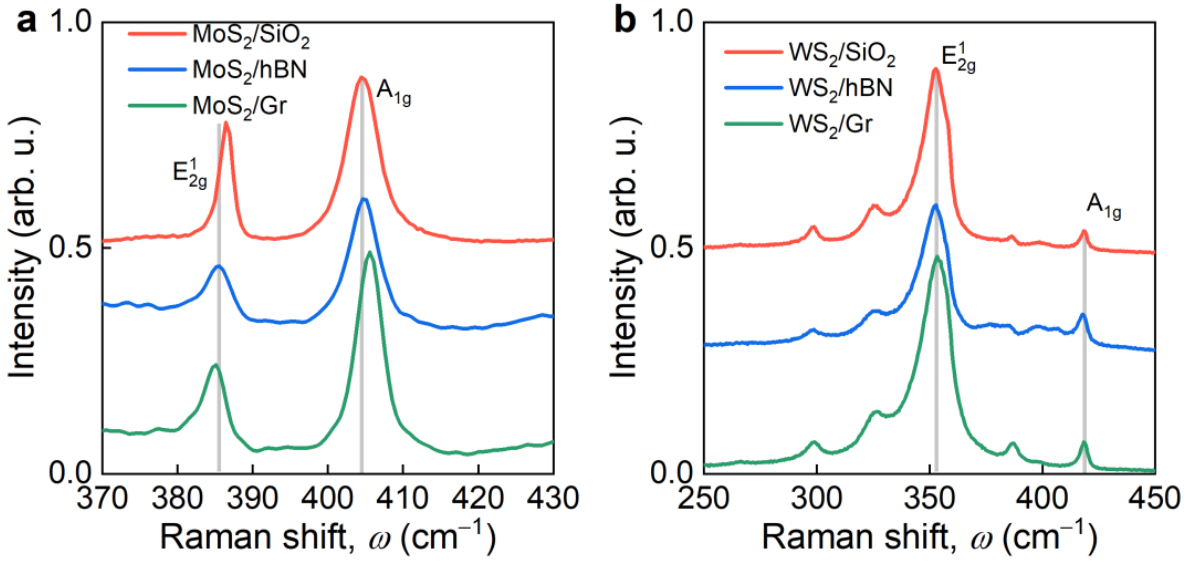

Figure 2. Raman spectra of (**a**) MoS_2 and (**b**) WS_2 in heterostructures. Grey lines are guidelines for eyes.

3.2. Non-Additive Optical Effects in Optical Constants

The dielectric response of 2D MoS_2 in heterostructures was investigated using spectroscopic ellipsometry. A four-layer model (air/MoS_2/Gr/SiO_2/Si and air/MoS_2/hBN/SiO_2/Si) was employed to retrieve an optical response of the MoS_2 monolayer in heterostructures from ellipsometry spectra (Figures A1 and A2). In the first step, we performed preliminary ellipsometry analysis, in particular, estimation of silicon oxide thickness. For this purpose, we fitted SiO_2 thickness within the additive optical model for heterostructures. It gave 11.9, 11.8, 317.9, and 328.0 nm SiO_2 thicknesses for the MoS_2/Gr, MoS_2/hBN, WS_2/Gr, and WS_2/hBN heterostructures, respectively. Afterward, we utilized point-by-point fitting [56,57] and then proceeded with the Tauc–Lorentz (TL) oscillator model to adequately describe the MoS_2 excitons (see Section 2) [46,47]. In accordance with the Raman results, optical constants of MoS_2 show a dramatic change in heterostructures (Figure 3). First, fundamental A- and B-excitons have lower oscillator strength in MoS_2/hBN and MoS_2/Gr heterostructures relative to pristine MoS_2, although peak positions remain the same. These observations can be explained by the change of dielectric environment, which is known to strongly modify transition metal dichalcogenides (TMDCs) excitons [58–60]. Moreover, a recent study [61] established a charge transfer in MoS_2/Gr, which can explain changes for A- and B-excitons since it could be considered as doping, which is known to modify A- and B-excitons [57]. For high-order MoS_2 excitons, the situation is more intriguing since they alter not only oscillator strength in MoS_2/hBN and MoS_2/Gr heterostructures, but also their position, and doping does not affect them [57]. These changes manifest in substantial difference in the refractive index (Figure 3a) and extinction coefficient (Figure 3b) of MoS_2 above 3 eV. Moreover, in the MoS_2/Gr case, we detected an additional excitonic peak around 3.5 eV (Figure 3b). This exciton has previously been observed for MoS_2 in the presence of organic molecules, turning dark (light-inaccessible) excitons into bright ones

(light-accessible) [47,62]. By analogy, we assumed that it is similar for our scenario, except that, instead of organic molecules, it is graphene that assists in turning a dark exciton into a bright one. Additionally, Figures A1 and A2 compare of the non-additive (modified optical response of MoS_2 by heterostructure) and additive (pristine optical response of MoS_2) optical models, which show that both methods can be implemented up to 3 eV. Nonetheless, the non-additive model far more accurately captures the experimental results above 3 eV. Therefore, we drew the conclusion that MoS_2/Gr and MoS_2/hBN heterostructures can be viewed as independent layers for low-energy photons (<3 eV), whereas vdW interaction needs to be taken into consideration for high-energy photons (>3 eV).

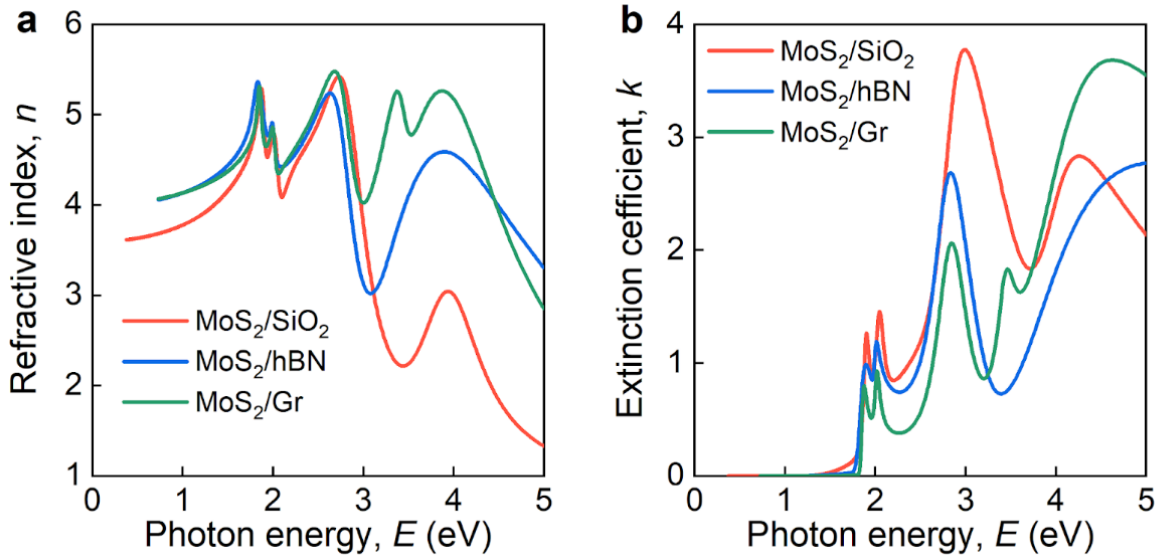

Figure 3. Optical constants of monolayer MoS_2 in heterostructures. (**a**) Refractive index and (**b**) extinction coefficient.

Similar to MoS_2 heterostructures (see Section 2, we determined the optical constants of WS_2 in the WS_2/Gr and WS_2/hBN heterostructures (Figure 4) from ellipsometry spectra (Figures A3 and A4). However, in contrast to MoS_2, the refractive index (Figure 4a) and extinction coefficient (Figure 4b) of WS_2 demonstrate slight alterations, compared to pristine WS_2. These observations are consistent with Raman findings (Figure 2b). Furthermore, if we take the original optical constants of WS_2 to calculate ellipsometric parameters Ψ and Δ, then they will be close to the measured one, as seen from Figures A3 and A4. Thus, although non-additive effects are present in WS_2 heterostructures (Figure 4), the additive optical model retains high predictive capability. Hence, for computations of WS_2 heterostructures in photonic devices, one can use both additive and non-additive optical models.

Apart from ellipsometry measurements, we also measured reflectance (Figure 5) of all heterostructures for unambiguous verification of found optical response, presented in Figures 3 and 4. From Figure 5, we clearly see a good agreement between experimental and transfer matrix [63] calculated spectra. They additionally proved our conclusions about modified optical response of MoS_2 and WS_2 in heterostructures.

Finally, to illustrate the practical significance of observed modifications in the optical properties of TMDCs in the heterostructures, we theoretically studied a biosensor based on the surface plasmon resonance (SPR). To improve characteristics of the biosensor, we covered the surface of gold with a periodical MoS_2/Gr heterostructure. Here, MoS_2 is employed as a high-index material, whereas the topmost graphene sheet can serve as an effective linking layer [64,65]. We found that the optical sensitivity of the SPR biosensor is enhanced by deposition of the MoS_2/Gr heterostructure, reaching as high as 167 deg/RIU with three added bilayers (Figure 6b). At the same time, the use of additive (unchanged) optical constants leads to a 4% lower optical sensitivity of 160 deg/RIU. In addition, the resonance dip position and magnitude depend on the optical properties of MoS_2 (Figure 6a).

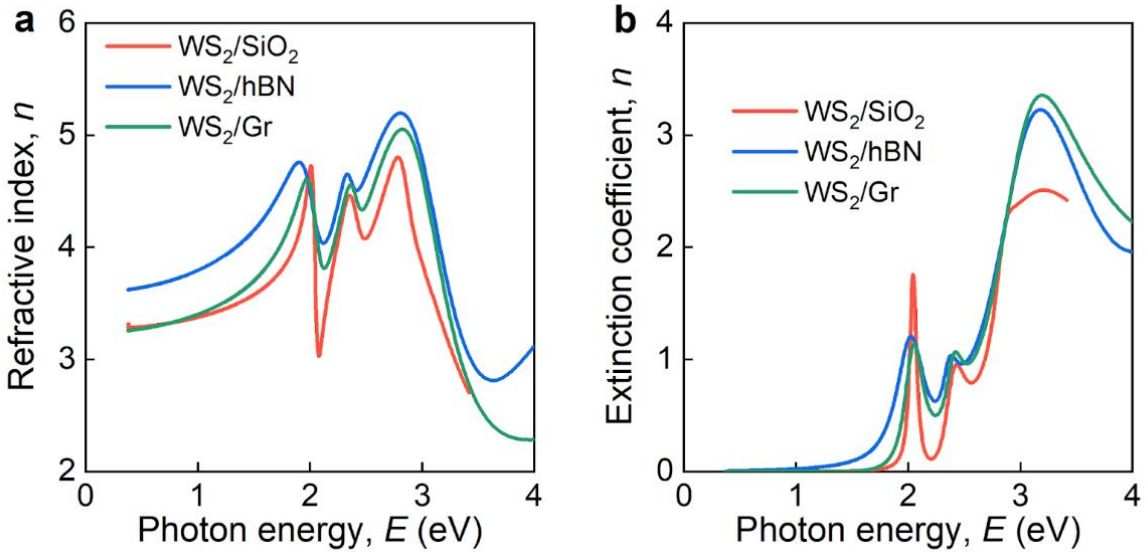

Figure 4. Optical constants of monolayer WS_2 in heterostructures. (**a**) Refractive index and (**b**) extinction coefficient.

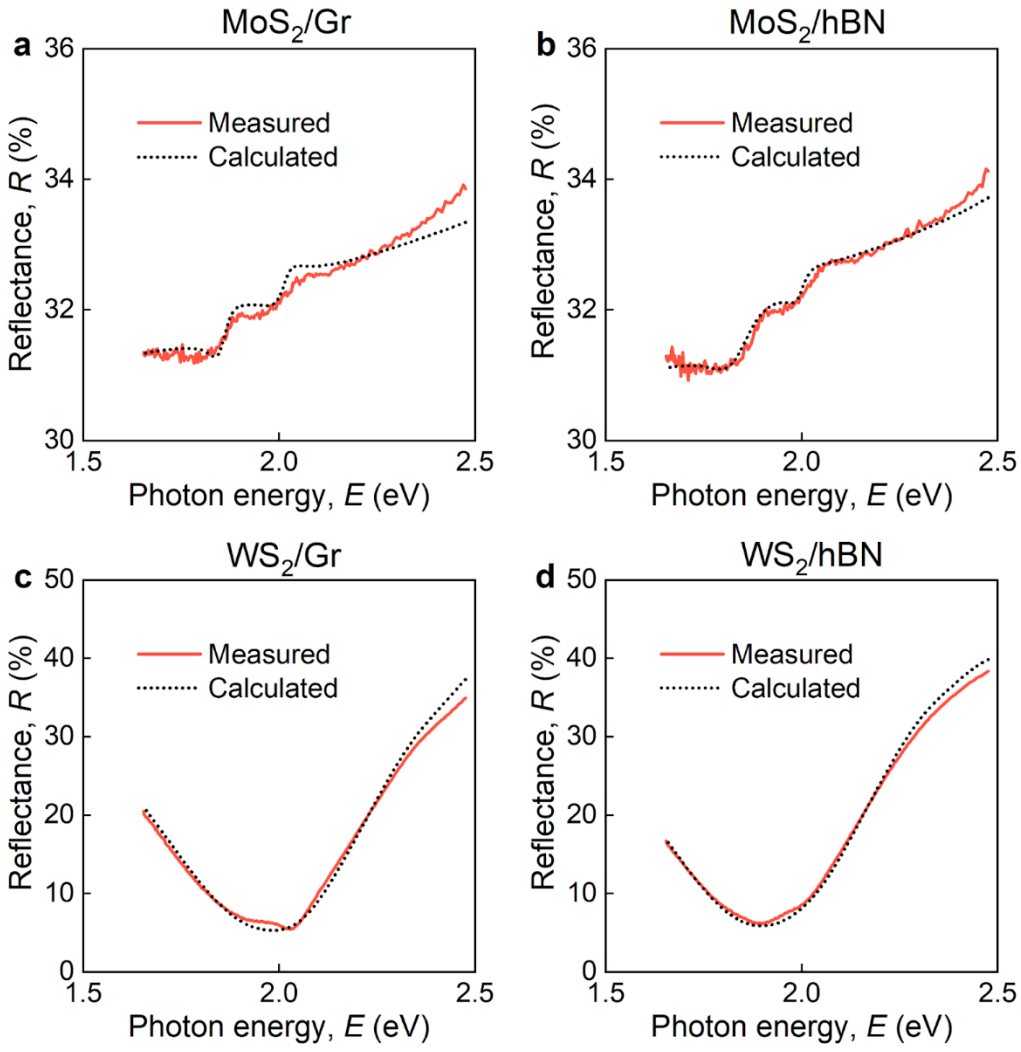

Figure 5. Measured and calculated reflectance spectra for (**a**) MoS_2/Gr, (**b**) MoS_2/hBN, (**c**) WS_2/Gr, and (**d**) WS_2/hBN heterostructures.

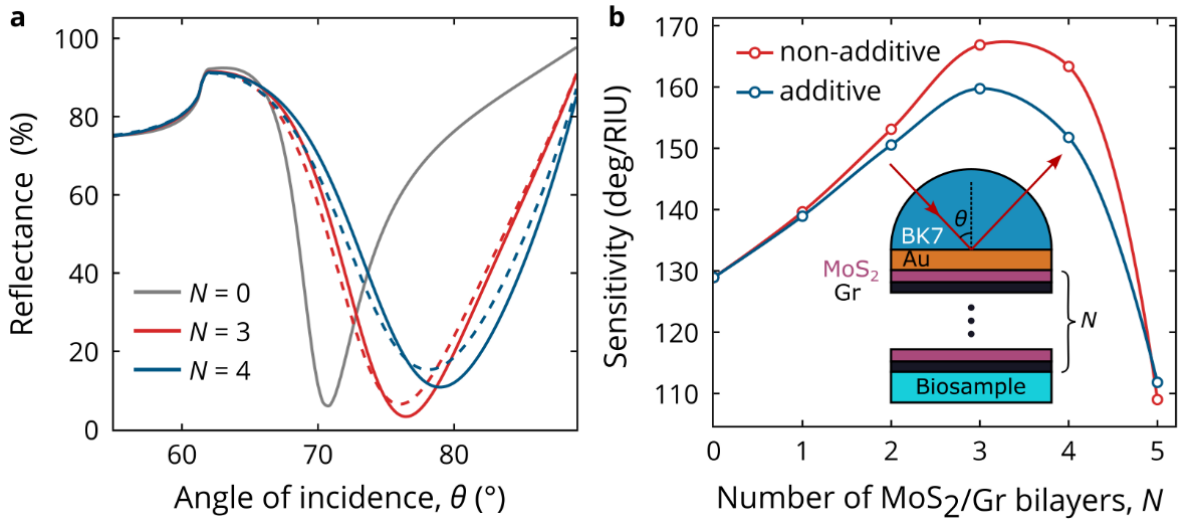

Figure 6. SPR biosensor performance. (**a**) Angle-resolved reflectance for different number N of MoS_2/Gr bilayers deposited on gold layer. Dashed and solid lines were calculated using the additive and non-additive dielectric functions of MoS_2, correspondingly. (**b**) Angular sensitivity of the biosensor as a function of N calculated with the additive (blue line) and non-additive (red line) dielectric functions of MoS_2. Inset: schematic view of the studied biosensor. The thickness of gold is 40 nm, and the operating wavelength is 635 nm.

4. Conclusions

To summarize, we investigated the optical response of van der Waals (vdW) heterostructures on the example of MoS_2/Gr, MoS_2/hBN, WS_2/Gr, and WS_2/hBN. We observed a noticeable change in excitonic optical response in two-dimensional (2D) MoS_2 and WS_2, attributed to vdW interaction between layers in heterostructures. In detail, excitons in MoS_2 demonstrate not only modification in oscillator strength, but also peak position shift and emergence of new excitonic peaks, resulting from a dark (light-inaccessible) to bright (light-accessible) exciton switch in the presence of graphene. On the other hand, excitons in WS_2 show alterations only in oscillator strength and broadening, suggesting a different vdW interaction between Gr and hBN with MoS_2 and WS_2. Hence, our results indicate nontrivial influence of heterostructures on optical constants, which may be used to manipulate the optical response of vdW photonic [66–68] and optoelectronic [69–71] elements. Finally, it gives a positive answer to the question about non-additive effects of vdW heterostructures on the dielectric function of 2D materials. It offers an indispensable degree of freedom for photonic engineers, but complicates the computation of vdW heterostructures' optical performance since each vdW configuration has a unique optical response, which does not decompose into individual monolayer responses.

Author Contributions: V.S.V., A.V.A., A.A.V. and G.A.E. suggested and directed the project. M.A.E.-S., A.P.T., G.A.E., M.K.T., D.I.Y., A.S.S. and S.M.N. performed the measurements and analyzed the data. G.A.E. and A.A.V. provided theoretical support. M.A.E.-S., A.P.T., G.A.E., A.A.V., A.V.A. and V.S.V. contributed to the interpretation of the experimental results. G.A.E. wrote the original draft. G.A.E., A.P.T. and M.A.E.-S. contributed equally to this work and should be considered the first co-authors. All authors reviewed and edited the paper. All authors contributed to the discussions and commented on the paper. All authors have read and agreed to the published version of the manuscript.

Funding: This work was supported by the Russian Science Foundation (grant no. 22-19-00558). G.A.E. was supported by the Fellowship of the President of the Russian Federation to young scientists and postgraduates (SP-2627.2021.5).

Data Availability Statement: The data presented in this study are available upon reasonable request from the corresponding author.

Acknowledgments: The authors thank the MIPT's Shared Research Facilities Center for the use of their equipment.

Conflicts of Interest: The authors declare no conflict of interest.

Appendix A

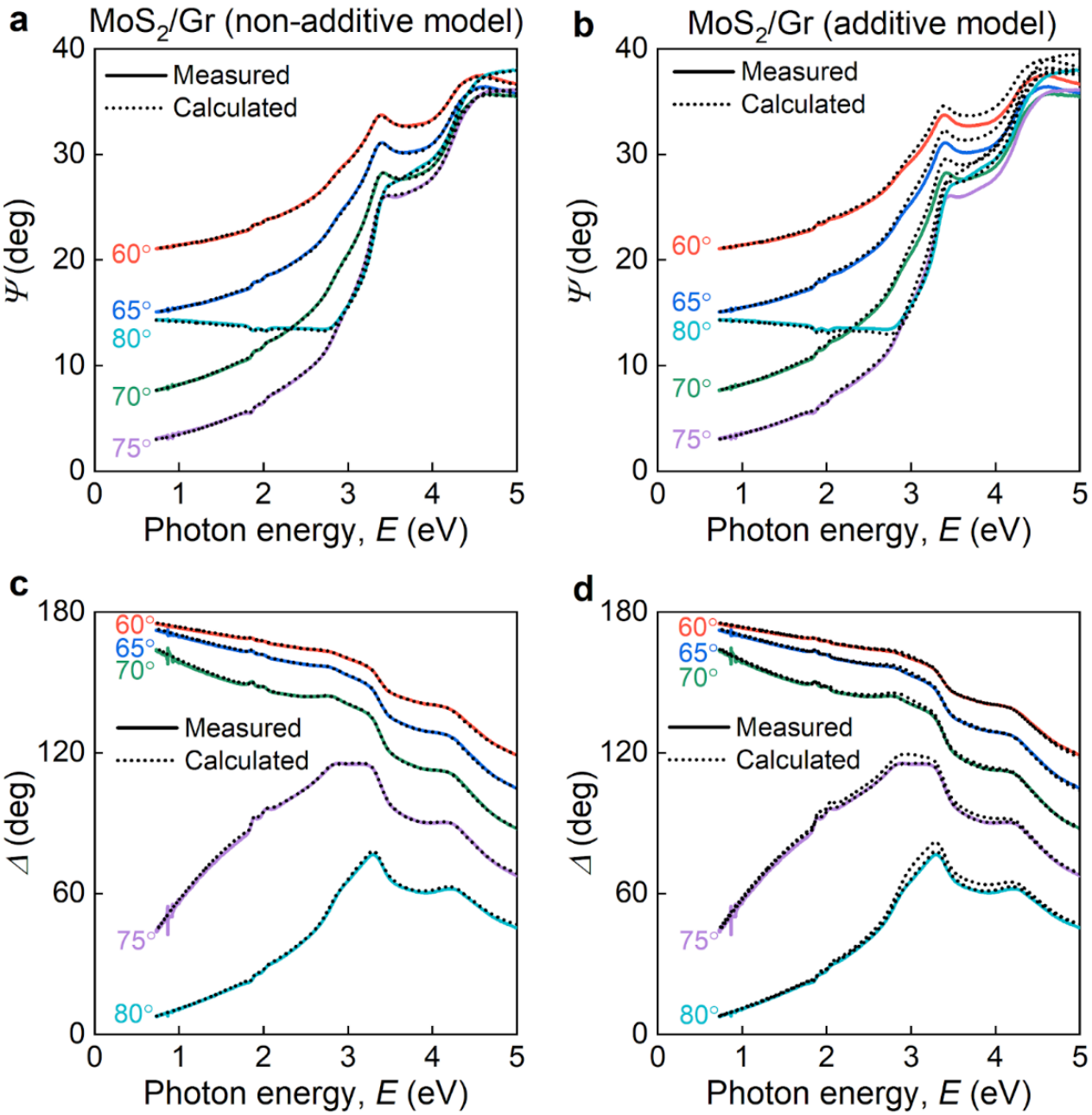

Figure A1. Ellipsometry spectra of MoS_2/Gr heterostructures. Comparison of non-additive and additive optical models for (**a**,**b**) Ψ and (**c**,**d**) Δ. Red, blue, green, violet, and cyan lines correspond to 60°, 65°, 70°, 75°, and 80° incident angles, respectively.

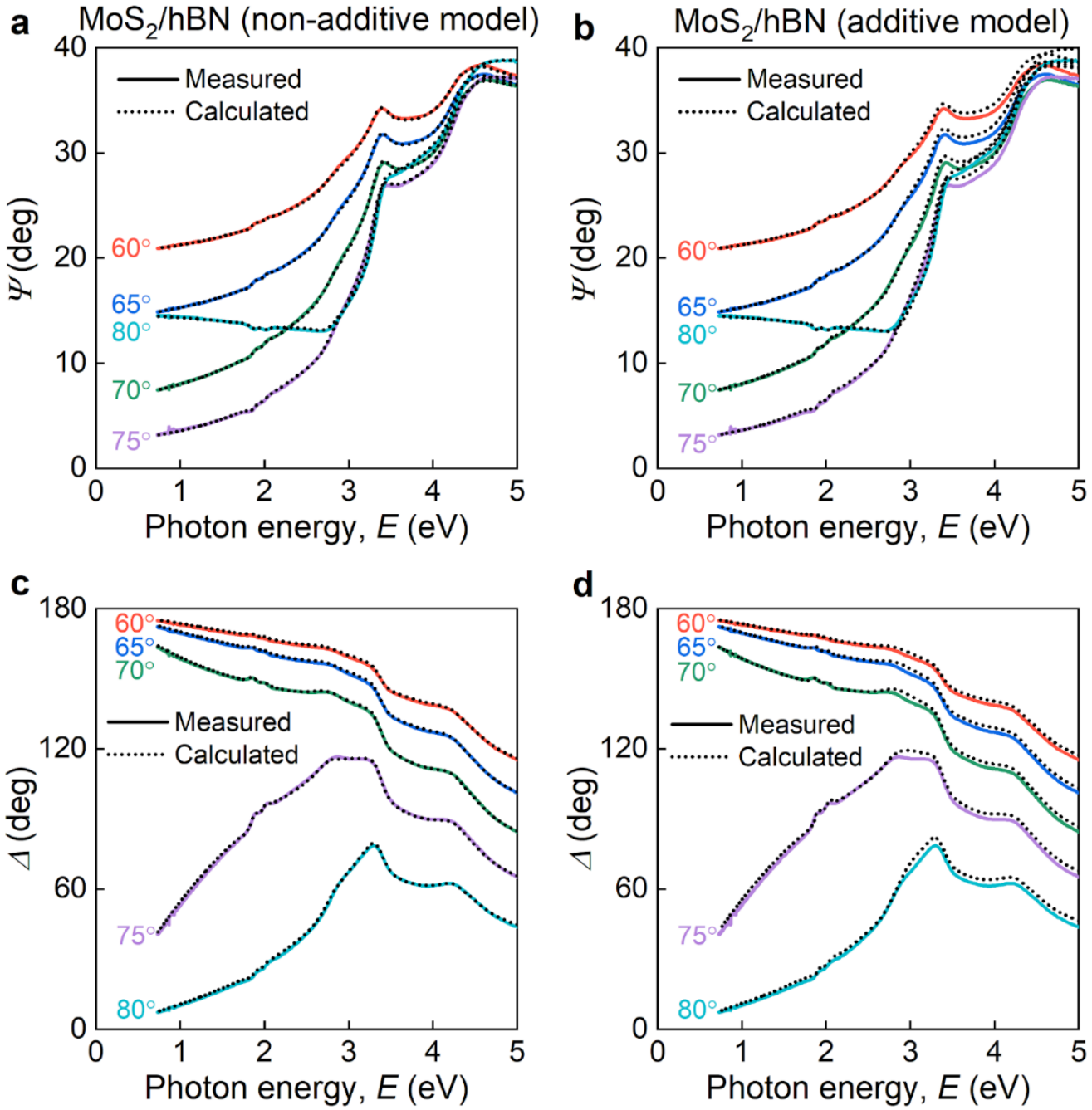

Figure A2. Ellipsometry spectra of MoS_2/hBN heterostructures. Comparison of non-additive and additive optical models for (**a**,**b**) Ψ and (**c**,**d**) Δ. Red, blue, green, violet, and cyan lines correspond to 60°, 65°, 70°, 75°, and 80° incident angles, respectively.

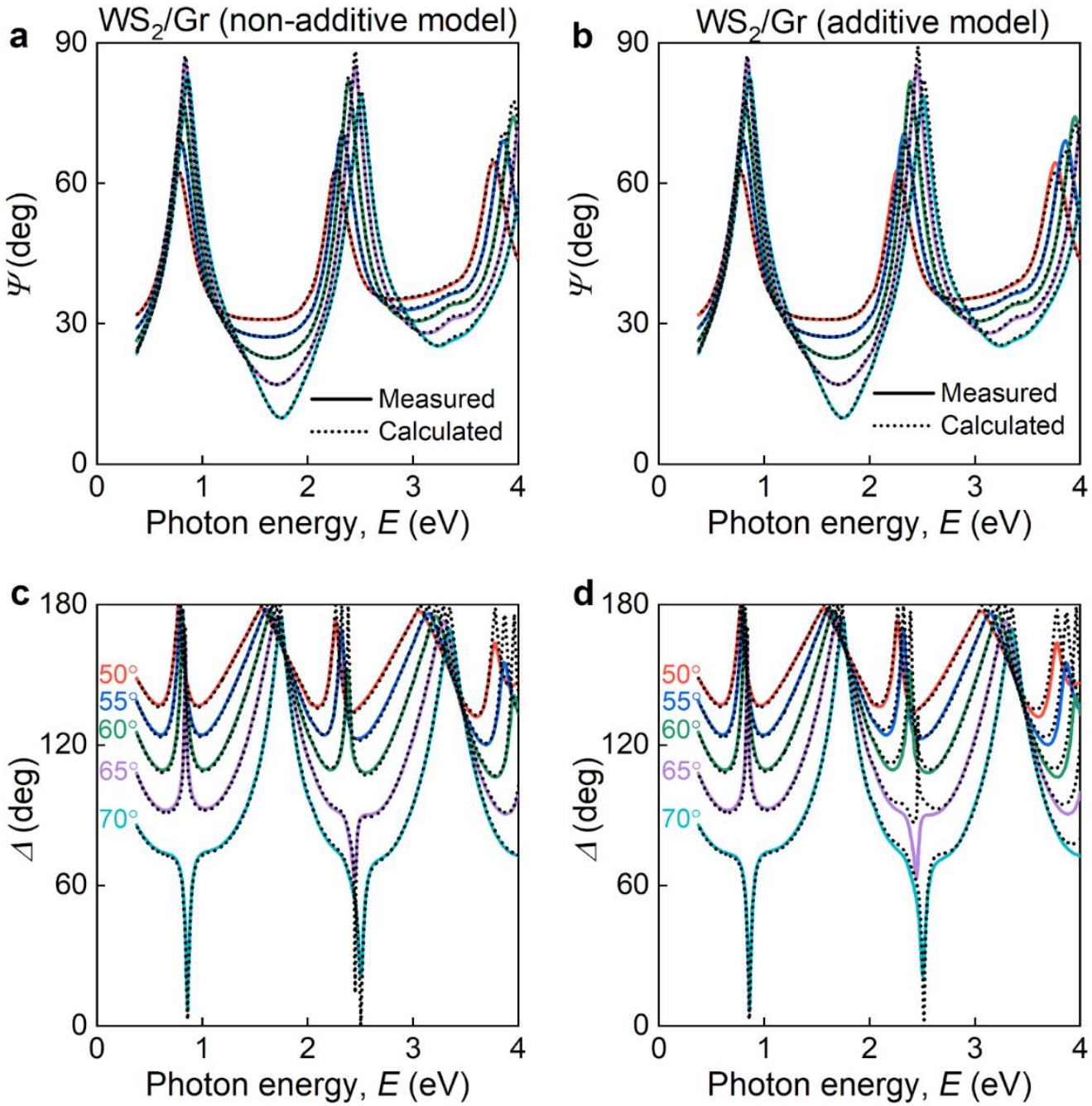

Figure A3. Ellipsometry spectra of WS_2/Gr heterostructures. Comparison of non-additive and additive optical models for (**a**,**b**) Ψ and (**c**,**d**) Δ. Red, blue, green, violet, and cyan lines correspond to 50°, 55°, 60°, 65°, and 70° incident angles, respectively.

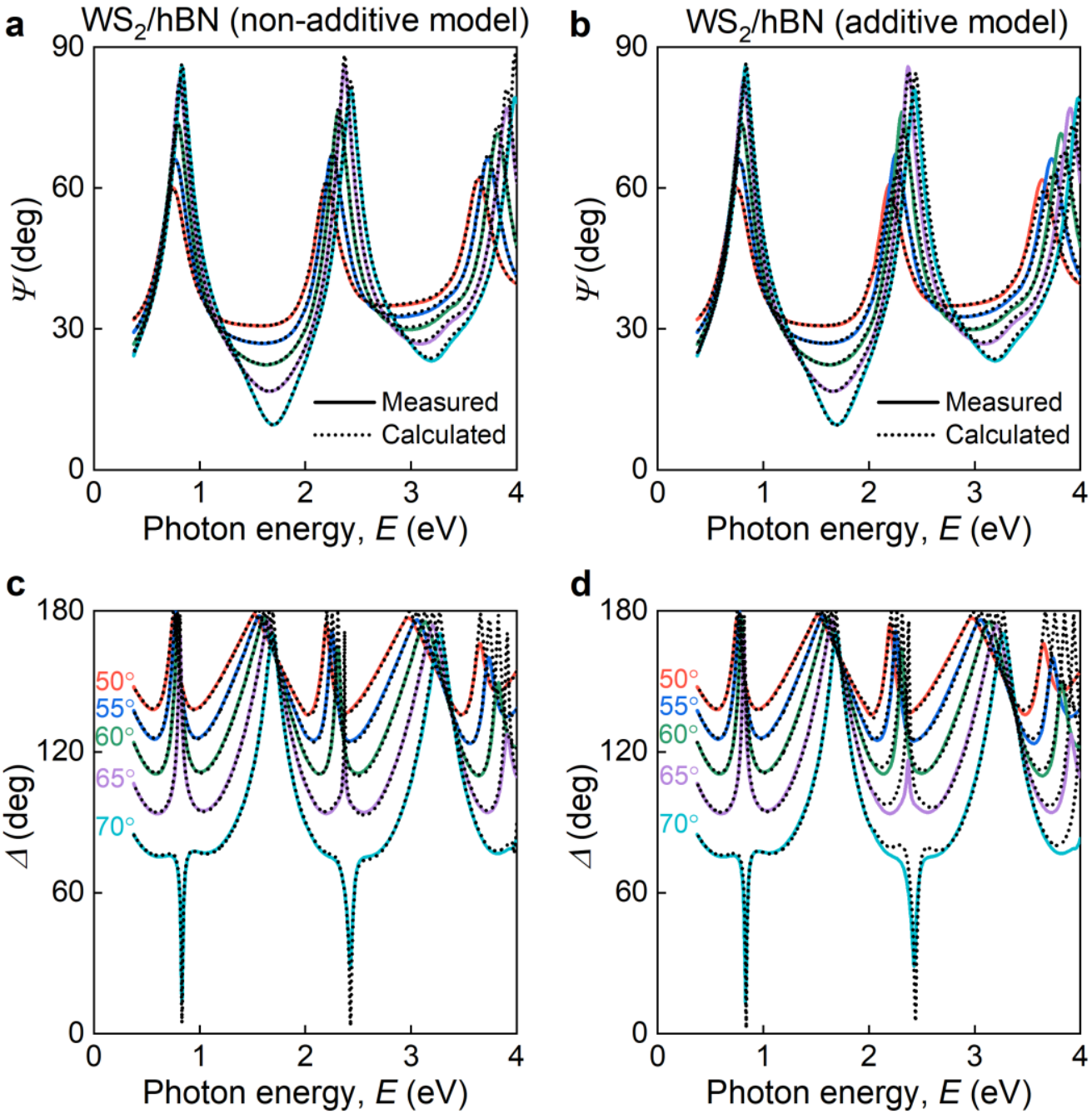

Figure A4. Ellipsometry spectra of WS_2/hBN heterostructures. Comparison of non-additive and additive optical models for (**a**,**b**) Ψ and (**c**,**d**) Δ. Red, blue, green, violet, and cyan lines correspond to 50°, 55°, 60°, 65°, and 70° incident angles, respectively.

References

1. Lamberti, C.; Agostini, G. *Characterization of Semiconductor Heterostructures and Nanostructures*; Elsevier: Amsterdam, The Netherlands, 2013; ISBN 978-0-444-59551-5.
2. Alferov, Z.I. The History and Future of Semiconductor Heterostructures. *Semiconductors* **1998**, *32*, 1–14. [CrossRef]
3. Smith, A.M.; Nie, S. Semiconductor Nanocrystals: Structure, Properties, and Band Gap Engineering. *Acc. Chem. Res.* **2010**, *43*, 190–200. [CrossRef] [PubMed]
4. Ning, C.-Z.; Dou, L.; Yang, P. Bandgap Engineering in Semiconductor Alloy Nanomaterials with Widely Tunable Compositions. *Nat. Rev. Mater.* **2017**, *2*, 17070. [CrossRef]
5. Son, J.; Moetakef, P.; Jalan, B.; Bierwagen, O.; Wright, N.J.; Engel-Herbert, R.; Stemmer, S. Epitaxial $SrTiO_3$ Films with Electron Mobilities Exceeding 30,000 $Cm^2\ V^{-1}\ S^{-1}$. *Nat. Mater.* **2010**, *9*, 482–484. [CrossRef] [PubMed]

6. Trier, F.; Christensen, D.V.; Pryds, N. Electron Mobility in Oxide Heterostructures. *J. Phys. D Appl. Phys.* **2018**, *51*, 293002. [CrossRef]
7. Koval, O.Y.; Fedorov, V.V.; Bolshakov, A.D.; Fedina, S.V.; Kochetkov, F.M.; Neplokh, V.; Sapunov, G.A.; Dvoretckaia, L.N.; Kirilenko, D.A.; Shtrom, I.V.; et al. Structural and Optical Properties of Self-Catalyzed Axially Heterostructured GaPN/GaP Nanowires Embedded into a Flexible Silicone Membrane. *Nanomaterials* **2020**, *10*, 2110. [CrossRef] [PubMed]
8. Fedorov, V.V.; Koval, O.Y.; Ryabov, D.R.; Fedina, S.V.; Eliseev, I.E.; Kirilenko, D.A.; Pidgayko, D.A.; Bogdanov, A.A.; Zadiranov, Y.M.; Goltaev, A.S.; et al. Nanoscale Gallium Phosphide Epilayers on Sapphire for Low-Loss Visible Nanophotonics. *ACS Appl. Nano Mater.* **2022**, *5*, 8846–8858. [CrossRef]
9. Wang, Y.; Mambakkam, S.V.; Huang, Y.-X.; Wang, Y.; Ji, Y.; Xiao, C.; Yang, S.A.; Law, S.A.; Xiao, J.Q. Observation of Nonlinear Planar Hall Effect in Magnetic-Insulator–Topological-Insulator Heterostructures. *Phys. Rev. B* **2022**, *106*, 155408. [CrossRef]
10. Khmelevskaia, D.; Markina, D.I.; Fedorov, V.V.; Ermolaev, G.A.; Arsenin, A.V.; Volkov, V.S.; Goltaev, A.S.; Zadiranov, Y.M.; Tzibizov, I.A.; Pushkarev, A.P.; et al. Directly Grown Crystalline Gallium Phosphide on Sapphire for Nonlinear All-Dielectric Nanophotonics. *Appl. Phys. Lett.* **2021**, *118*, 201101. [CrossRef]
11. Chang, L.L.; Ploog, K. *Molecular Beam Epitaxy and Heterostructures*; Chang, L.L., Ploog, K., Eds.; Springer: Dordrecht, The Netherlands, 1985; ISBN 978-94-010-8744-5.
12. Koma, A. Summary Abstract: Fabrication of Ultrathin Heterostructures with van Der Waals Epitaxy. *J. Vac. Sci. Technol. B Microelectron. Nanom. Struct.* **1985**, *3*, 724. [CrossRef]
13. Choudhury, T.H.; Zhang, X.; Al Balushi, Z.Y.; Chubarov, M.; Redwing, J.M. Epitaxial Growth of Two-Dimensional Layered Transition Metal Dichalcogenides. *Annu. Rev. Mater. Res.* **2020**, *50*, 155–177. [CrossRef]
14. Ermolaev, G.A.; El-Sayed, M.A.; Yakubovsky, D.I.; Voronin, K.V.; Romanov, R.I.; Tatmyshevskiy, M.K.; Doroshina, N.V.; Nemtsov, A.B.; Voronov, A.A.; Novikov, S.M.; et al. Optical Constants and Structural Properties of Epitaxial MoS_2 Monolayers. *Nanomaterials* **2021**, *11*, 1411. [CrossRef] [PubMed]
15. Hutzler, A.; Fritsch, B.; Matthus, C.D.; Jank, M.P.M.; Rommel, M. Highly Accurate Determination of Heterogeneously Stacked Van-Der-Waals Materials by Optical Microspectroscopy. *Sci. Rep.* **2020**, *10*, 13676. [CrossRef] [PubMed]
16. Frisenda, R.; Niu, Y.; Gant, P.; Molina-Mendoza, A.J.; Schmidt, R.; Bratschitsch, R.; Liu, J.; Fu, L.; Dumcenco, D.; Kis, A.; et al. Micro-Reflectance and Transmittance Spectroscopy: A Versatile and Powerful Tool to Characterize 2D Materials. *J. Phys. D Appl. Phys.* **2017**, *50*, 074002. [CrossRef]
17. Geim, A.K.; Grigorieva, I.V. Van Der Waals Heterostructures. *Nature* **2013**, *499*, 419–425. [CrossRef]
18. Novoselov, K.S.; Mishchenko, A.; Carvalho, A.; Castro Neto, A.H. 2D Materials and van Der Waals Heterostructures. *Science* **2016**, *353*, aac9439. [CrossRef]
19. Liu, Y.; Weiss, N.O.; Duan, X.; Cheng, H.-C.; Huang, Y.; Duan, X. Van Der Waals Heterostructures and Devices. *Nat. Rev. Mater.* **2016**, *1*, 16042. [CrossRef]
20. Yankowitz, M.; Ma, Q.; Jarillo-Herrero, P.; LeRoy, B.J. Van Der Waals Heterostructures Combining Graphene and Hexagonal Boron Nitride. *Nat. Rev. Phys.* **2019**, *1*, 112–125. [CrossRef]
21. Dean, C.R.; Young, A.F.; Meric, I.; Lee, C.; Wang, L.; Sorgenfrei, S.; Watanabe, K.; Taniguchi, T.; Kim, P.; Shepard, K.L.; et al. Boron Nitride Substrates for High-Quality Graphene Electronics. *Nat. Nanotechnol.* **2010**, *5*, 722–726. [CrossRef]
22. Wang, L.; Meric, I.; Huang, P.Y.; Gao, Q.; Gao, Y.; Tran, H.; Taniguchi, T.; Watanabe, K.; Campos, L.M.; Muller, D.A.; et al. One-Dimensional Electrical Contact to a Two-Dimensional Material. *Science* **2013**, *342*, 614–617. [CrossRef]
23. Halbertal, D.; Finney, N.R.; Sunku, S.S.; Kerelsky, A.; Rubio-Verdú, C.; Shabani, S.; Xian, L.; Carr, S.; Chen, S.; Zhang, C.; et al. Moiré Metrology of Energy Landscapes in van Der Waals Heterostructures. *Nat. Commun.* **2021**, *12*, 242. [CrossRef] [PubMed]
24. Shimazaki, Y.; Schwartz, I.; Watanabe, K.; Taniguchi, T.; Kroner, M.; Imamoğlu, A. Strongly Correlated Electrons and Hybrid Excitons in a Moiré Heterostructure. *Nature* **2020**, *580*, 472–477. [CrossRef] [PubMed]
25. Jin, C.; Regan, E.C.; Yan, A.; Iqbal Bakti Utama, M.; Wang, D.; Zhao, S.; Qin, Y.; Yang, S.; Zheng, Z.; Shi, S.; et al. Observation of Moiré Excitons in WSe_2/WS_2 Heterostructure Superlattices. *Nature* **2019**, *567*, 76–80. [CrossRef] [PubMed]
26. Fitzgerald, J.M.; Thompson, J.J.P.; Malic, E. Twist Angle Tuning of Moiré Exciton Polaritons in van Der Waals Heterostructures. *Nano Lett.* **2022**, *22*, 4468–4474. [CrossRef] [PubMed]
27. Dong, R.; Jacob, A.; Bourdais, S.; Sanvito, S. High-Throughput Bandstructure Simulations of van Der Waals Hetero-Bilayers Formed by 1T and 2H Monolayers. *npj 2D Mater. Appl.* **2021**, *5*, 26. [CrossRef]
28. Zhao, X.; Shi, Z.; Wang, X.; Zou, H.; Fu, Y.; Zhang, L. Band Structure Engineering through van Der Waals Heterostructing Superlattices of two-dimensional Transition Metal Dichalcogenides. *InfoMat* **2021**, *3*, 201–211. [CrossRef]
29. Kunstmann, J.; Mooshammer, F.; Nagler, P.; Chaves, A.; Stein, F.; Paradiso, N.; Plechinger, G.; Strunk, C.; Schüller, C.; Seifert, G.; et al. Momentum-Space Indirect Interlayer Excitons in Transition-Metal Dichalcogenide van Der Waals Heterostructures. *Nat. Phys.* **2018**, *14*, 801–805. [CrossRef]
30. Nagler, P.; Mooshammer, F.; Kunstmann, J.; Ballottin, M.V.; Mitioglu, A.; Chernikov, A.; Chaves, A.; Stein, F.; Paradiso, N.; Meier, S.; et al. Interlayer Excitons in Transition-Metal Dichalcogenide Heterobilayers. *Phys. Status Solidi* **2019**, *256*, 1900308. [CrossRef]
31. Cao, Y.; Fatemi, V.; Fang, S.; Watanabe, K.; Taniguchi, T.; Kaxiras, E.; Jarillo-Herrero, P. Unconventional Superconductivity in Magic-Angle Graphene Superlattices. *Nature* **2018**, *556*, 43–50. [CrossRef]

32. Park, J.M.; Cao, Y.; Xia, L.-Q.; Sun, S.; Watanabe, K.; Taniguchi, T.; Jarillo-Herrero, P. Robust Superconductivity in Magic-Angle Multilayer Graphene Family. *Nat. Mater.* **2022**, *21*, 877–883. [CrossRef]
33. Aggoune, W.; Cocchi, C.; Nabok, D.; Rezouali, K.; Belkhir, M.A.; Draxl, C. Structural, Electronic, and Optical Properties of Periodic Graphene/h-BN van Der Waals Heterostructures. *Phys. Rev. Mater.* **2020**, *4*, 084001. [CrossRef]
34. Abergel, D.S.L.; Wallbank, J.R.; Chen, X.; Mucha-Kruczyński, M.; Fal'ko, V.I. Infrared Absorption by Graphene–HBN Heterostructures. *New J. Phys.* **2013**, *15*, 123009. [CrossRef]
35. Qiu, B.; Zhao, X.; Hu, G.; Yue, W.; Ren, J.; Yuan, X. Optical Properties of Graphene/MoS_2 Heterostructure: First Principles Calculations. *Nanomaterials* **2018**, *8*, 962. [CrossRef] [PubMed]
36. Farkous, M.; Bikerouin, M.; Phung, H.T.T.; El-Yadri, M.; Feddi, E.; Dujardin, F.; Duque, C.A.; Muoi, D.; Phuc, H.V.; Nguyen, C.V.; et al. Electronic and Optical Properties of Layered van Der Waals Heterostructure Based on MS_2 (M = Mo, W) Monolayers. *Mater. Res. Express* **2019**, *6*, 065060. [CrossRef]
37. Ma, Y.; Lu, S.; Dong, X.; Han, G.; Chen, Z.; Liu, Y. Optical Parameters of Graphene/MoS_2 van Der Waals Heterostructure Investigated by Spectroscopic Ellipsometry. *Appl. Surf. Sci.* **2022**, *599*, 153987. [CrossRef]
38. Toksumakov, A.; Ermolaev, G.; Tatmyshevskiy, M.; Klishin, Y.; Slavich, A.; Begichev, I.; Stosic, D.; Yakubovsky, D.; Kvashnin, D.; Vyshnevyy, A.; et al. Anomalous Optical Response of Graphene on Hexagonal Boron Nitride Substrates. *arXiv* **2022**. [CrossRef]
39. Hsu, C.; Frisenda, R.; Schmidt, R.; Arora, A.; Vasconcellos, S.M.; Bratschitsch, R.; Zant, H.S.J.; Castellanos-Gomez, A. Thickness-Dependent Refractive Index of 1L, 2L, and 3L MoS_2, $MoSe_2$, WS_2, and WSe_2. *Adv. Opt. Mater.* **2019**, *7*, 1900239. [CrossRef]
40. Yoo, S.; Park, Q.-H. Spectroscopic Ellipsometry for Low-Dimensional Materials and Heterostructures. *Nanophotonics* **2022**, *11*, 2811–2825. [CrossRef]
41. Cai, Z.; Liu, B.; Zou, X.; Cheng, H.M. Chemical Vapor Deposition Growth and Applications of Two-Dimensional Materials and Their Heterostructures. *Chem. Rev.* **2018**, *118*, 6091–6133. [CrossRef]
42. Gurarslan, A.; Yu, Y.; Su, L.; Yu, Y.; Suarez, F.; Yao, S.; Zhu, Y.; Ozturk, M.; Zhang, Y.; Cao, L. Surface-Energy-Assisted Perfect Transfer of Centimeter-Scale Monolayer and Few-Layer MoS_2 Films onto Arbitrary Substrates. *ACS Nano* **2014**, *8*, 11522–11528. [CrossRef]
43. Herzinger, C.M.; Johs, B.; McGahan, W.A.; Woollam, J.A.; Paulson, W. Ellipsometric Determination of Optical Constants for Silicon and Thermally Grown Silicon Dioxide via a Multi-Sample, Multi-Wavelength, Multi-Angle Investigation. *J. Appl. Phys.* **1998**, *83*, 3323–3336. [CrossRef]
44. El-Sayed, M.A.; Ermolaev, G.A.; Voronin, K.V.; Romanov, R.I.; Tselikov, G.I.; Yakubovsky, D.I.; Doroshina, N.V.; Nemtsov, A.B.; Solovey, V.R.; Voronov, A.A.; et al. Optical Constants of Chemical Vapor Deposited Graphene for Photonic Applications. *Nanomaterials* **2021**, *11*, 1230. [CrossRef] [PubMed]
45. Segura, A.; Artús, L.; Cuscó, R.; Taniguchi, T.; Cassabois, G.; Gil, B. Natural Optical Anisotropy of H-BN: Highest Giant Birefringence in a Bulk Crystal through the Mid-Infrared to Ultraviolet Range. *Phys. Rev. Mater.* **2018**, *2*, 024001. [CrossRef]
46. Ermolaev, G.A.; Yakubovsky, D.I.; Stebunov, Y.V.; Arsenin, A.V.; Volkov, V.S. Spectral Ellipsometry of Monolayer Transition Metal Dichalcogenides: Analysis of Excitonic Peaks in Dispersion. *J. Vac. Sci. Technol. B* **2020**, *38*, 014002. [CrossRef]
47. Ermolaev, G.A.; Stebunov, Y.V.; Vyshnevyy, A.A.; Tatarkin, D.E.; Yakubovsky, D.I.; Novikov, S.M.; Baranov, D.G.; Shegai, T.; Nikitin, A.Y.; Arsenin, A.V.; et al. Broadband Optical Properties of Monolayer and Bulk MoS_2. *npj 2D Mater. Appl.* **2020**, *4*, 21. [CrossRef]
48. Niu, Y.; Gonzalez-Abad, S.; Frisenda, R.; Marauhn, P.; Drüppel, M.; Gant, P.; Schmidt, R.; Taghavi, N.; Barcons, D.; Molina-Mendoza, A.; et al. Thickness-Dependent Differential Reflectance Spectra of Monolayer and Few-Layer MoS_2, $MoSe_2$, WS_2 and WSe_2. *Nanomaterials* **2018**, *8*, 725. [CrossRef]
49. Zhang, S.; Li, B.; Chen, X.; Ruta, F.L.; Shao, Y.; Sternbach, A.J.; McLeod, A.S.; Sun, Z.; Xiong, L.; Moore, S.L.; et al. Nano-Spectroscopy of Excitons in Atomically Thin Transition Metal Dichalcogenides. *Nat. Commun.* **2022**, *13*, 542. [CrossRef]
50. Castellanos-Gomez, A.; Duan, X.; Fei, Z.; Gutierrez, H.R.; Huang, Y.; Huang, X.; Quereda, J.; Qian, Q.; Sutter, E.; Sutter, P. Van Der Waals Heterostructures. *Nat. Rev. Methods Prim.* **2022**, *2*, 58. [CrossRef]
51. Ermolaev, G.; Voronin, K.; Baranov, D.G.; Kravets, V.; Tselikov, G.; Stebunov, Y.; Yakubovsky, D.; Novikov, S.; Vyshnevyy, A.; Mazitov, A.; et al. Topological Phase Singularities in Atomically Thin High-Refractive-Index Materials. *Nat. Commun.* **2022**, *13*, 2049. [CrossRef]
52. Ermolaev, G.A.; Voronin, K.V.; Tatmyshevskiy, M.K.; Mazitov, A.B.; Slavich, A.S.; Yakubovsky, D.I.; Tselin, A.P.; Mironov, M.S.; Romanov, R.I.; Markeev, A.M.; et al. Broadband Optical Properties of Atomically Thin PtS_2 and $PtSe_2$. *Nanomaterials* **2021**, *11*, 3269. [CrossRef]
53. Ermolaev, G.A.; Yakubovsky, D.I.; El-Sayed, M.A.; Tatmyshevskiy, M.K.; Mazitov, A.B.; Popkova, A.A.; Antropov, I.M.; Bessonov, V.O.; Slavich, A.S.; Tselikov, G.I.; et al. Broadband Optical Constants and Nonlinear Properties of SnS_2 and $SnSe_2$. *Nanomaterials* **2021**, *12*, 141. [CrossRef] [PubMed]
54. Cong, X.; Liu, X.-L.; Lin, M.-L.; Tan, P.-H. Application of Raman Spectroscopy to Probe Fundamental Properties of Two-Dimensional Materials. *npj 2D Mater. Appl.* **2020**, *4*, 13. [CrossRef]
55. Paillet, M.; Parret, R.; Sauvajol, J.-L.; Colomban, P. Graphene and Related 2D Materials: An Overview of the Raman Studies. *J. Raman Spectrosc.* **2018**, *49*, 8–12. [CrossRef]
56. Yu, Y.; Yu, Y.; Cai, Y.; Li, W.; Gurarslan, A.; Peelaers, H.; Aspnes, D.E.; Van de Walle, C.G.; Nguyen, N.V.; Zhang, Y.-W.; et al. Exciton-Dominated Dielectric Function of Atomically Thin MoS_2 Films. *Sci. Rep.* **2015**, *5*, 16996. [CrossRef] [PubMed]

57. Kravets, V.G.; Wu, F.; Auton, G.H.; Yu, T.; Imaizumi, S.; Grigorenko, A.N. Measurements of Electrically Tunable Refractive Index of MoS_2 Monolayer and Its Usage in Optical Modulators. *npj 2D Mater. Appl.* **2019**, *3*, 36. [CrossRef]
58. Rösner, M.; Steinke, C.; Lorke, M.; Gies, C.; Jahnke, F.; Wehling, T.O. Two-Dimensional Heterojunctions from Nonlocal Manipulations of the Interactions. *Nano Lett.* **2016**, *16*, 2322–2327. [CrossRef]
59. Raja, A.; Chaves, A.; Yu, J.; Arefe, G.; Hill, H.M.; Rigosi, A.F.; Berkelbach, T.C.; Nagler, P.; Schüller, C.; Korn, T.; et al. Coulomb Engineering of the Bandgap and Excitons in Two-Dimensional Materials. *Nat. Commun.* **2017**, *8*, 15251. [CrossRef]
60. Raja, A.; Waldecker, L.; Zipfel, J.; Cho, Y.; Brem, S.; Ziegler, J.D.; Kulig, M.; Taniguchi, T.; Watanabe, K.; Malic, E.; et al. Dielectric Disorder in Two-Dimensional Materials. *Nat. Nanotechnol.* **2019**, *14*, 832–837. [CrossRef]
61. De Luna Bugallo, A.; Rocha-Robledo, A.K.; Flores-Salazar, M.; Muñiz-Martinez, B.A.; Cerda-Méndez, E.A.; Del Pozo-Zamudio, O.; Jiménez-Sandoval, S.; Rosales-Torres, Á.A.; Lara-Alfaro, H.F. Interlayer Charge Transfer in Supported and Suspended MoS_2/Graphene/MoS_2 Vertical Heterostructures. *SSRN Electron. J.* **2022**. [CrossRef]
62. Feierabend, M.; Berghäuser, G.; Knorr, A.; Malic, E. Proposal for Dark Exciton Based Chemical Sensors. *Nat. Commun.* **2017**, *8*, 14776. [CrossRef]
63. Passler, N.C.; Paarmann, A. Generalized 4 × 4 Matrix Formalism for Light Propagation in Anisotropic Stratified Media: Study of Surface Phonon Polaritons in Polar Dielectric Heterostructures. *J. Opt. Soc. Am. B* **2017**, *34*, 2128. [CrossRef]
64. Wu, B.; Mathews, N.; Sum, T.-C. *Plasmonic Organic Solar Cells*; Springer: Singapore, 2017; ISBN 978-981-10-2021-6.
65. Stebunov, Y.V.; Aftenieva, O.A.; Arsenin, A.V.; Volkov, V.S. Highly Sensitive and Selective Sensor Chips with Graphene-Oxide Linking Layer. *ACS Appl. Mater. Interfaces* **2015**, *7*, 21727–21734. [CrossRef] [PubMed]
66. Lin, H.; Xu, Z.-Q.; Cao, G.; Zhang, Y.; Zhou, J.; Wang, Z.; Wan, Z.; Liu, Z.; Loh, K.P.; Qiu, C.-W.; et al. Diffraction-Limited Imaging with Monolayer 2D Material-Based Ultrathin Flat Lenses. *Light Sci. Appl.* **2020**, *9*, 137. [CrossRef] [PubMed]
67. Xia, F.; Wang, H.; Xiao, D.; Dubey, M.; Ramasubramaniam, A. Two-Dimensional Material Nanophotonics. *Nat. Photonics* **2014**, *8*, 899–907. [CrossRef]
68. Ermolaev, G.; Grudinin, D.; Voronin, K.; Vyshnevyy, A.; Arsenin, A.; Volkov, V. Van Der Waals Materials for Subdiffractional Light Guidance. *Photonics* **2022**, *9*, 744. [CrossRef]
69. Bandurin, D.A.; Mönch, E.; Kapralov, K.; Phinney, I.Y.; Lindner, K.; Liu, S.; Edgar, J.H.; Dmitriev, I.A.; Jarillo-Herrero, P.; Svintsov, D.; et al. Cyclotron Resonance Overtones and Near-Field Magnetoabsorption via Terahertz Bernstein Modes in Graphene. *Nat. Phys.* **2022**, *18*, 462–467. [CrossRef]
70. Asgari, M.; Riccardi, E.; Balci, O.; De Fazio, D.; Shinde, S.M.; Zhang, J.; Mignuzzi, S.; Koppens, F.H.L.; Ferrari, A.C.; Viti, L.; et al. Chip-Scalable, Room-Temperature, Zero-Bias, Graphene-Based Terahertz Detectors with Nanosecond Response Time. *ACS Nano* **2021**, *15*, 17966–17976. [CrossRef]
71. Quereda, J.; Kuriakose, S.; Munuera, C.; Mompean, F.J.; Al-Enizi, A.M.; Nafady, A.; Diez, E.; Frisenda, R.; Castellanos-Gomez, A. Scalable and Low-Cost Fabrication of Flexible WS_2 Photodetectors on Polycarbonate. *npj Flex. Electron.* **2022**, *6*, 23. [CrossRef]